Chapter 8
Monte Carlo and Molecular Dynamics Simulations of Clay Mineral Systems

Evgeniy M. Myshakin and Randall T. Cygan

Abstract This chapter is focused on reviewing molecular dynamics and Monte Carlo simulations of greenhouse gases' interactions with swelling clay minerals. This chapter unfolds with the results of simulations on stepwise expansion of interlayer in hydrated montmorillonite. Next, an overview of the simulation data on carbon dioxide intercalation in clays is given with respect to structural changes, transport properties, thermodynamics, spectroscopic characteristics, sorption behavior at the basal clay surfaces, and surface wettability changes in CO_2-brine-mineral systems. Effects of the chemical nature of interlayer ions, as well as charge density and its distribution within clay layers on carbon dioxide/water intercalation and interaction with clay surfaces, are discussed. Then, results of methane interaction with hydrated swelling clays are presented. The discussion is centered around the formation of gas hydrate phase in the interlayer under suitable pressure and temperature conditions. Dynamic nature of hydrate cages encapsulating methane molecules is considered together with a mechanism of their formation in interlayer. A shift of the equilibrium pressure and temperature conditions in comparison with bulk phase is attributed to distortion of hydrate lattice in clay and to finite pore space. Finally, intercalation of the carbon dioxide/methane molecules in interlayer is reviewed through competitive adsorption of the binary mixture on clay surfaces.

Before considering intercalation of greenhouse gases into the interlayer of swelling clay minerals, it is important to realize that such processes can only occur in hydrated systems (refer to Chap. 7). The experimental (Chaps. 6 and 7) and theoretical (Cygan, Guggenheim, & Koster van Groos, 2004a; Botan et al., 2010; Makaremi, Jordan, Guthrie, & Myshakin, 2015; Rao & Leng, 2016a, b) studies indicate that water must be present in the interlayer for CO_2 and methane to be intercalated. It was already mentioned in Chap. 7 that the expansion of clay is

E. M. Myshakin (✉)
U.S. Department of Energy, NETL–AECOM, Pittsburgh, USA
e-mail: Evgeniy.Myshakin@netl.doe.gov

R. T. Cygan
U.S. Department of Energy, Sandia National Laboratories (SNL), Albuquerque, USA

V. Romanov (ed.), *Greenhouse Gases and Clay Minerals*, Green Energy and Technology, https://doi.org/10.1007/978-3-319-12661-6_8

governed by formation of the extended hydrogen-bonding network of water molecules among themselves, with clay surface and interlayer ions. Formation of the first fully developed hydration shell—enthalpies of hydration for sodium and calcium ions are −405 and −1592 kJ/mol, respectively (Burgess, 1999)—around interlayer ions is a leading factor promoting the expansion (Young & Smith, 2000). Carbon dioxide and methane are ineffective solvents of the counter-balancing ions to make the swelling be thermodynamically favorable; so, it requires at least residual amount of water to prop open the interlayer space.

CO_2 and CH_4 retaining in the interlayer space are in equilibrium with surrounding bulk mobile phase in pore and interstitial (between clay particles) regions, and their interlayer concentrations are larger compared with saturated concentrations in water-rich bulk phase at prevailing pressure and temperature conditions. At typical conditions of deep saline aquifers—340–350 K and 10–13 MPa, 800–1000 m below the surface (Benson & Cole, 2008)—a molar fraction of methane and carbon dioxide in liquid phase would be of the order of 10^{-4} and 10^{-2}–10^{-3}, respectively, according to the Peng-Robinson EoS (Huber, 2007). The predicted molar fraction of CO_2 in binary mixture with water in the interlayer at 1 W state of Na-exchanged montmorillonite and 100% relative humidity (RH) is around 0.06–0.12 (348.15 K/12.5 MPa) (Botan et al., 2010; Makaremi et al., 2015) and goes further up to 0.16 at 30% of RH (348 K/13 MPa) (Rao & Leng, 2016b). Injection of supercritical CO_2 into a geological reservoir would result in exposure of smectites (*i.e.*, swelling clay minerals) to CO_2-rich bulk phase, however that phase is unstable in the interlayer space of swelling clays and H_2O-rich one is realized (Schaef et al., 2015; Loring et al., 2014; Rother et al., 2013; Botan et al., 2010; Makaremi et al., 2015; Rao & Leng, 2016a, b). Schaef et al. (2015) and Loring et al. (2014) using a combination of *in situ* X-ray diffraction, infrared (IR) spectroscopic titrations, and quartz crystal microbalance measurements, estimated CO_2 adsorption at internal surface of montmorillonite (MMT). They found that at initial sub-1 W hydrate state of Ca-exchanged MMT exposed to supercritical CO_2 with undersaturated (10%) water concentration, CO_2 concentration in the interlayer can reach 0.8 mmol/g dry clay ($\sim$0.27 molar fraction in the interlayer; 50 °C and 9 MPa). As soon as water concentration in the interlayer increases producing a stepwise hydration profile, CO_2 concentration drops significantly.

Ji et al. (2012) performed a series of CH_4 adsorption experiments on clay-rich rocks conducted at 35–65 °C and at pressure up to 15 MPa under nearly dry conditions. They estimated the Langmuir volume of CH_4 normalized to clay minerals mass: MMT (0.48 mmol/g) > illite/smectite interstratified clay (0.41 mmol/g) > kaolinite (0.12 mmol/g) > chlorite (0.10 mmol/g) > illite (0.08 mmol/g). Assuming that part of adsorbed methane is entered the interlayer space of MMT and taking non-swelling kaolinite/chlorite/illite as a baseline, the internal adsorption of methane might be on an order of 0.4 mmol/g at sub-1 W initial d_{001}-spacings. Those data indicate that CO_2/CH_4 concentrations can reach appreciable values in interlayer space, so the intercalation mechanism provides a way to retain CO_2 and CH_4 in clay-rich geological formations under conditions of underground geologic aquifers or shale reservoirs. At pressure and temperature conditions of permafrost and deep marine

sediments, methane can be trapped in interlayer in a form of gas hydrate clathrate that can be thought as "double trapping" within confining environment of internal basal clay surfaces and additional immobilization is achieved within cages of hydrate lattice, that causes a sharp increase of trapped methane concentration that will be discussed later in this chapter.

The basal d_{001}-spacing of natural clays such as Na-MMT increases in a stepwise fashion with increasing RH that leads to change of an integral number of water layers (up to three, 1 W-3 W) in the interlayer space between adjacent clay layers. A comparison of d_{001}-spacing values from simulation with the corresponding experimental values (X-ray diffraction data) values serves as an excellent probe to validate the applicability of a particular force field to explore processes involving intercalation, dynamics, and transport properties of species in swelling clay minerals. Figure 8.1 reports the expansion of the d_{001}-spacing of Na-MMT upon water intercalation computed using molecular dynamics (MD) simulations with the Clayff force field (Cygan, Liang, & Kalinichev, 2004b). Comparison with experimental data (Fu, Zhang, & Low, 1990) shows that the MD results closely reproduce the experimental trend in the d_{001}-spacing, displaying plateaus corresponding to formation of monolayer and bilayer water arrangements in the interlayer. The spacing

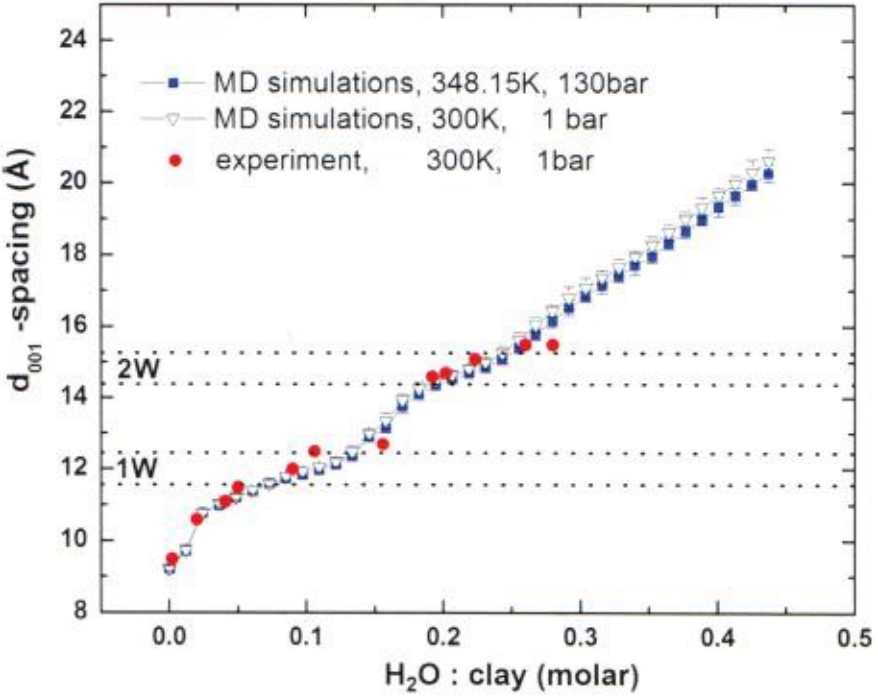

Fig. 8.1 Swelling behavior of Na-MMT upon hydration: *dotted lines* indicate the *d*-spacing ranges corresponding to stable hydration states—reprinted with permission from (Myshakin et al., 2013) Copyright (2013) American Chemical Society

curve calculated for the elevated pressure and temperature corresponding to underground conditions deviates only slightly from that calculated at 1 bar (10^5 Pa or 0.1 MPa) and 300 K. This finding is consistent with XRD measurements of d_{001}-spacing showing that hydration states are weekly dependent on pressure (Giesting, Guggenheim, Koster van Groos, & Busch, 2012b; Ilton et al., 2012) and brings confidence that MD simulations are capable to properly describe the processes of clay mineral expansion and intercalation.

8.1 Carbon Dioxide and Swelling Clay Minerals

Host rock matrix of the geological storage reservoirs used in the CO_2 sequestration (examined in the Chaps. 2 and 3) often includes swelling clay minerals able to intercalate carbon dioxide as a secondary trap, and which fueled a great deal of theoretical work aiming at understanding the molecular mechanisms of intercalation, thermodynamics, structural phenomena, and transport properties of intercalated species (Yang & Zaoui, 2016; Rao & Leng, 2016a, b; Kadoura, Nair, & Sun, 2016; Makaremi et al., 2015; Sena, Morrow, Kirkpatrick, & Krishnan, 2015; Myshakin et al., 2014; Lee, McGrail, & Glezakou, 2014; Myshakin et al., 2013; Cygan, Romanov, & Myshakin, 2012; Yang & Yang, 2011; Botan et al., 2010). Given the abundance of MMT in nature, it was often chosen as a typical swelling clay system and, particularly, Na- or Ca-MMT, which represent natural or Na-exchanged SWy MMT samples from Wyoming, and natural or Ca-exchanged STx MMT samples from Texas, respectively. The differences in chemical nature of interlayer counter-balancing ions and in distributions of isomorphic substitutions in clay layers can significantly affect the intercalation mechanism and will be considered below.

Figure 8.2 presents a schematic representation of tetrahedra (yellow)—octahedra (magenta/green)—tetrahedra (TOT) layer sequences of MMT with intercalated sodium ions, water and carbon dioxide molecules. The color alternation in the octahedral sheet represents the Al/Mg substitutions producing negative charge compensated by the interlayer ions.

Figure 8.3 displays *XY* and *XZ* planes of the internal basal surfaces (yellow tetrahedra in Fig. 8.2) in MMT exposed to the interlayer species. The silicon tetrahedra linked by shared basal oxygens form a periodic system of the hexagonal rings (the *XY* plane). Figure 8.2 depicts two types of interlayer ions; the first type represents surface-bound sodium ions adsorbed at the centers of the hexagonal rings (tetrahedral holes, Fig. 8.3) and coordinated to basal oxygens and oxygens of water molecules (inner-sphere complexes); and the second type is designated as ions fully coordinated to water molecules (outer-sphere complexes). The amount of water in the interlayer, layer charge distributions, and the chemical natures of the ions control the ratio of inner-to-outer sphere complexes (Rao & Leng, 2016a; Makaremi et al., 2015; Myshakin et al., 2013; Young & Smith, 2000). Intercalation of carbon dioxide disrupts the water network (Billemont, Coasne, & De Weireld,

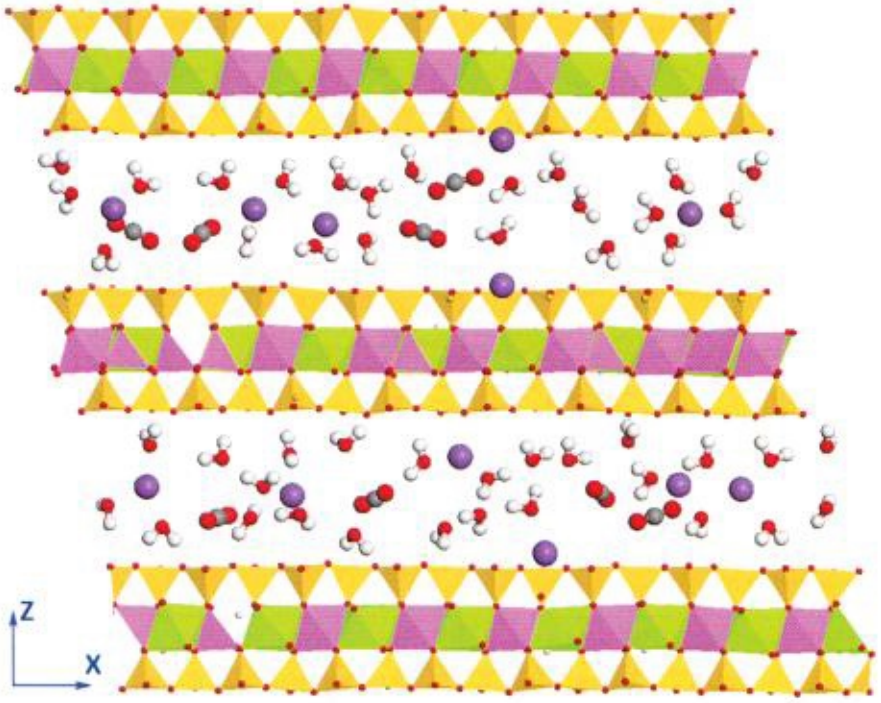

Fig. 8.2 Schematic representation of clay-water-CO_2 system; *Filled violet circle* = sodium ion, *Filled grey circle* = carbon, *Filled red circle* = oxygen, *Open circle* = hydrogen—reprinted with permission from (Myshakin et al., 2013) Copyright (2013) American Chemical Society

2010) and causes the Na^+ ions to be displaced toward the clay surfaces that, in turn, changes their relative wettability (Myshakin et al., 2013).

Classical molecular simulations of clay minerals rely on analytical expressions of potential energy to accurately describe the forces and energies associated with a statistical ensemble of atoms that comprise the clay-water or clay-CO_2 system. Accurate and flexible force fields for clay minerals (Teppen et al., 1997; Cygan et al., 2004b; Heinz, Lin, Mishra, & Emami, 2013) are available and can be implemented with specific H_2O models (SPC, TIP3P, etc.). Although involving nonflexible molecules or other constraints, several energy potentials for CO_2 are suitable for modeling gas, liquid, and supercritical states (Zhang & Duan, 2005; Aimoli, Maginn, & Abreu, 2014). Flexible CO_2 potentials that incorporate bond stretch and bond bend modes are particularly valuable in the analysis of interfaces such as the intercalation and adsorption of CO_2 in clay mineral systems (Harris & Yung, 1995; Zhu, Zhang, Liu, & Zhang, 2009; Cygan et al., 2012). Accurate and reliable force fields are critical in providing realistic molecular dynamics and Monte Carlo simulations, especially when the clay-fluid systems are comprised of many thousands to millions of atoms when quantum chemical methods would be computationally expensive.

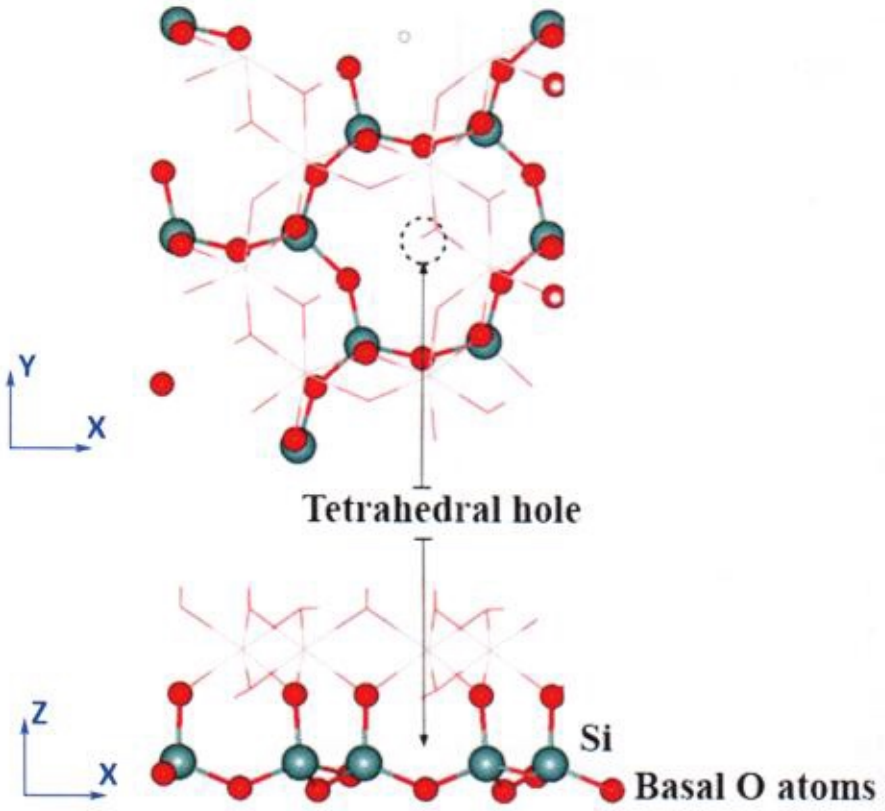

Fig. 8.3 Chemical structure of internal basal surface in smectite clay minerals. The upper *XY* projection shows the centers of hexagonal rings—reprinted with permission from (Michalkova & Tunega, 2007) Copyright (2007) American Chemical Society

In the molecular simulations, TOT layers are assumed to be perfectly oriented, although rotational disorder (in which layers may have different rotations with respect to the normal axis to the clay layer) inherently present in natural samples and manifests itself through turbostratically stacked clay layers (Viani, Gualtieri, & Artioli, 2002; Lutterotti et al., 2010). As a result, instead of having a coherent alignment of hexagonal rings on either side of the interlayer region, rotational disorder results in a Moiré pattern with a periodic variation in alignment of hexagonal rings across the interlayer. At sub-1 W hydration state, the formation of disordered clay layers is energetically favorable driven by electrostatic avoidance of cations adsorbed at the opposite internal surfaces (at the centers of the hexagonal rings). With increase of the interlayer space caused by water and carbon dioxide intercalation, disordering becomes an energetically demanding process (Myshakin et al., 2014).

Figure 8.4 demonstrates the d_{001}-spacing calculated as a function of the number of water molecules for selected numbers of intercalated carbon dioxide molecules per unit cell. The bottom curve, which displays expansion in the absence of carbon

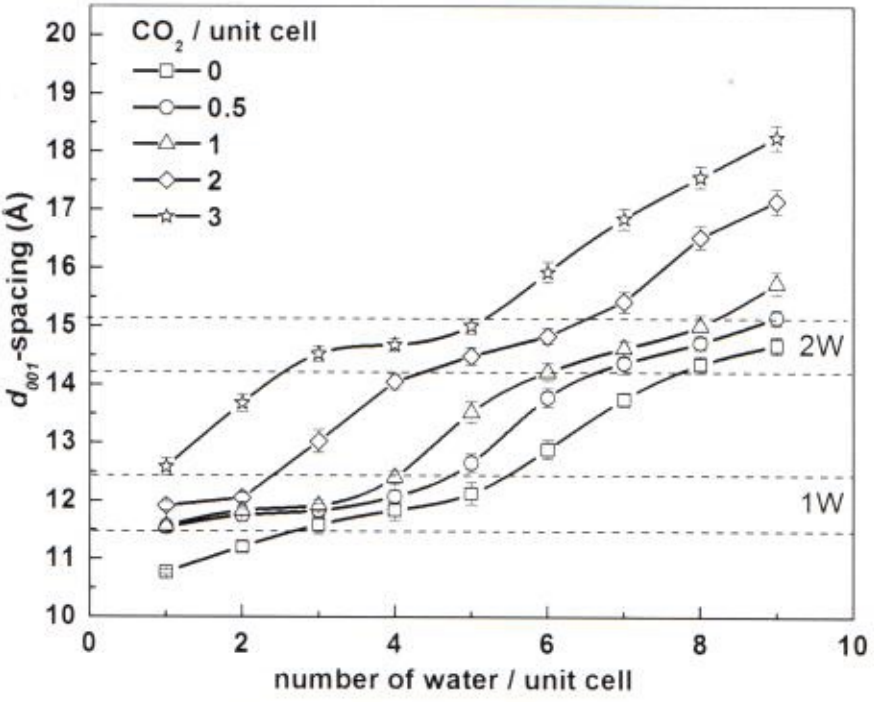

Fig. 8.4 d_{001}-spacing as a function of the number of water molecules at fixed numbers of CO_2 molecules per unit cell: *dashed lines* indicate ranges of basal d_{001}-spacing corresponding to 1W and 2 W hydration states—reprinted with permission from (Myshakin et al., 2013) Copyright (2013) American Chemical Society

dioxide molecules, serves as the reference. The most important observation deduced from these simulations is that introduction of CO_2 into interlayer does not change the characteristic stepwise swelling. Carbon dioxide mainly affects the transition from 1 W to 2 W by shifting it to smaller water amount with an increase of carbon dioxide concentration. It is also interesting to note that water-CO_2 compositions like 8–0.5, 7–1, and 6–2 all demonstrate similar d_{001}-spacings. As a result, the process of CO_2 intercalation can be accompanied by displacement of water molecules while keeping d_{001}-spacing nearly constant rather than further expanding the interlayer spacing. The analysis of atomistic distributions reported by different groups reveal that in CO_2/H_2O monolayer and bilayer, carbon dioxide molecules tend to orient parallel to the clay basal surface (Rao & Leng, 2016b; Kadoura et al., 2016; Makaremi et al., 2015; Sena et al., 2015; Myshakin et al., 2013; Botan et al., 2010). Moreover, with concentration increase, CO_2 (due to its hydrophobic nature) forms clusters/agglomerations in the interlayer facilitating lateral diffusion through percolation pathways (Rao & Leng, 2016b; Sena et al., 2015; Myshakin et al., 2014).

Examination of these clusters has showed that most of the pairs of near-neighbor CO_2 molecules adopt a slipped parallel coordination geometry with respect to each

other while a small fraction displays a tilted T-shaped geometry (Rao & Leng, 2016b; Sena et al., 2015) in line with orientation configuration of CO_2 dimers in supercritical state (Cipriani, Nardone, Ricci, & Ricci, 2001; Saharay & Balasubramanian, 2004a, b; Saharay & Balasubramanian, 2006). Water molecules preferentially form first hydration shells around interlayer ions although the corresponding coordination numbers are lower because of steric hindrance—imposed by the confining environment of the clay layers (for outer-sphere complexes at 1 W state) and ion adsorption at the surfaces with basal oxygens participating in solvation (for inner-sphere complexes)—to add up to the coordination number corresponding to bulk water (Rao & Leng, 2016b; Makaremi et al., 2015). Water molecules that are not part of a hydration shell around interlayer ions also interact with intercalated CO_2 molecules. Infrared spectroscopic measurements have shown that trapping of carbon dioxide in Na- and Ca-MMT leads to a red shift in the asymmetric fundamental stretch frequency of the CO_2 molecule (Romanov, 2013; Hur et al., 2013). DFT-based MD simulations carried out to explain the origin of this red shift identify the electric field of water dipoles mainly responsible for induced elongation of the CO bonds of CO_2 and the observed frequency shift (Myshakin et al., 2013). In other words, the extent of the shift depends on the amount of intercalated water and could serve as a preliminary probe to a hydration state to supplement XRD measurements of d_{001}-spacings.

Transport properties of interlayer species were examined by many researchers focusing on estimation of self-diffusion coefficients of carbon dioxide, water, and ions in the direction parallel to the internal basal surfaces (Yang & Zaoui, 2016; Rao & Leng, 2016b; Kadoura et al., 2016; Makaremi et al., 2015; Sena et al., 2015; Lee et al., 2014; Myshakin et al., 2013; Cygan et al., 2012; Yang & Yang, 2011; Botan et al., 2010). As a general consensus, the presence of CO_2 retards the diffusion of water and counter-balancing ions. The diffusion of H_2O and Na^+ in the presence of CO_2 for the monolayer (1 W) is about 2.5 times smaller than in the absence of CO_2 and 1.5 times for the bilayer (2 W) (Botan et al., 2010). The tendency of CO_2 molecules to form clusters and lack of participation in solvation of interlayer ions result in higher diffusion coefficients than those of water molecules and interlayer ions (Rao & Leng, 2016b). The most retarded motion is estimated for the interlayer ions experiencing strong electrostatic interactions with charged clay layers. As a result, total diffusion of the counter-balancing cations should be separated into contributions from surface-bound cations and those forming outer-sphere complexes (Myshakin et al., 2013).

To estimate the amount of intercalated carbon dioxide in the interlayer, Monte Carlo (MC) simulations are a convenient tool that also provides access to thermodynamics of the swelling process (Rao & Leng, 2016a, b; Makaremi et al., 2015; Botan et al., 2010). Figure 8.5 displays computed free energy of clay swelling due to intercalation of H_2O/CO_2 mixture in Na-MMT and Na-beidellite as a function of d_{001}-spacing. The MMT clay model bears charge in the central octahedral sheets, which is screened from direct exposure to interlayer species by the tetrahedral sheets. In contrast, the beidellite model carries charge in the tetrahedral sheets that allow the study of the effect of negative charge locations on the swelling behavior.

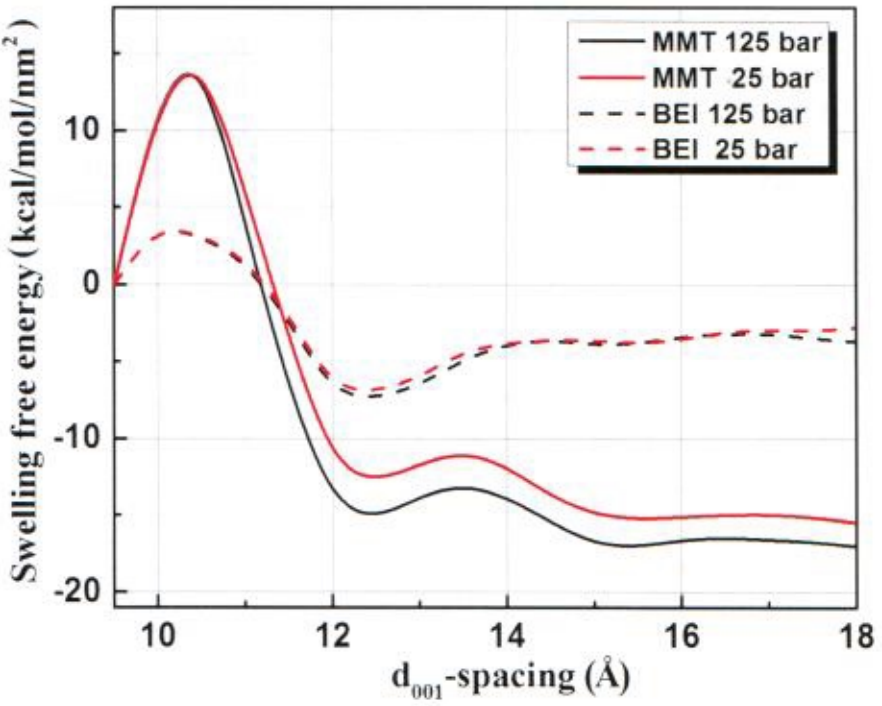

Fig. 8.5 Calculated swelling free energy of Na-MMT and Na-beidellite as a function of d-spacing for intercalation of H_2O-CO_2 mixture at P = 25 and 125 bar, T = 348.15 K—reprinted with permission from (Makaremi et al., 2015) Copyright (2015) American Chemical Society

Both clay systems have same charge ($-0.75e$) per unit cell compensated by sodium ions. The energy curves show that intercalation (starting from the dry clay) required to overcome the energy barriers followed by energy minima corresponding to 1 W (monolayer) and 2 W (bilayer) hydration states. An increase of pressure provides more defined free-energy minima and stabilization of the interlayer configurations. Figure 8.6 presents the CO_2 molar fraction in the intercalated H_2O/CO_2 mixture in equilibrium with bulk phase and corresponding to the swelling energies estimated at the d_{001}-spacing in Fig. 8.5. In both systems, there is a pronounced peak in the CO_2 mole fraction at a d_{001}-spacing corresponding to the 1 W state and a second weaker peak (or shoulder) at a distance corresponding to 2 W, in agreement with experiment showing that the maximum expansion of the interlayer due to CO_2 exposure occurs at the initial sub-1 W hydration state with residual amount of intercalated water (Giesting, Guggenheim, Koster van Groos, & Busch, 2012a, b; Loring et al., 2014; Schaef et al., 2015). The concentration of CO_2 in the interlayer region for both clay mineral systems substantially exceeds that in the bulk water-rich phase. Pressure increase causes an elevation of the intercalated CO_2 concentration. For Na-MMT, the calculated mole fractions of CO_2 in the interlayer region is in good

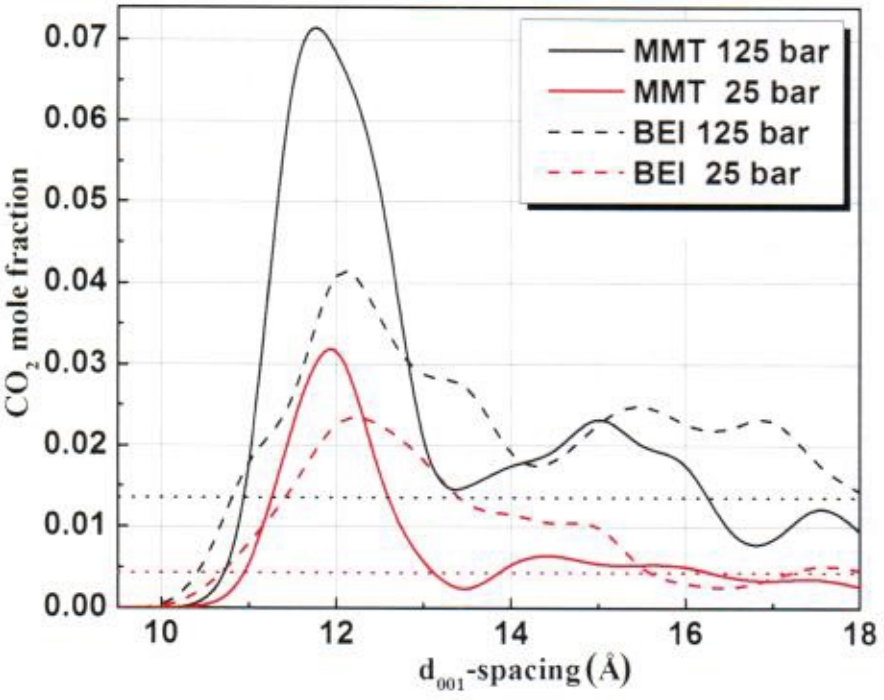

Fig. 8.6 CO_2 mole fraction in interlayer as a function of *d*-spacing for Na-MMT and Na-beidellite at P = 25 and 125 bar, T = 348.15 K. Horizontal *dotted lines* represent CO_2 mole fractions in bulk H_2O-rich phase at P = 25 and 125 bar, T = 348.15 K—reprinted with permission from (Makaremi et al., 2015) Copyright (2015) American Chemical Society

agreement with those reported by Botan et al. (2010) who used a different theoretical approach.

The charge localized at the tetrahedral sheets in beidellite decreases the ability of the interlayer to retain carbon dioxide relative to MMT that has negative charge localized in the octahedral sheets. Swelling free energy also demonstrates that the monolayer of the H_2O/CO_2 mixture is more stable in the interlayer of beidellite compared to MMT, which shows the greater stability of the bilayer (Fig. 8.5). The differences in stability of 1 W and 2 W states for hydrated MMT and beidellite (without CO_2) are documented in the literature and are attributed to specifics of ion solvation (Smith et al., 2004). Figure 8.7 depicts density profile distributions of the interlayer species for Na-MMT-H_2O-CO_2 and Na-beidellite-H_2O-CO_2 systems that provide insight into the relative stability of monolayer and bilayer mixture configurations. The density profiles confirm that carbon dioxide molecules form a mixture with water at monolayer (Fig. 8.7a) and bilayer (Fig. 8.7b) configurations. As a monolayer, the Na^+ distribution demonstrates two peaks for both MMT and beidellite. Due to stronger electrostatic interactions, the positions of the peaks are shifted more closely to the surfaces for beidellite. However, in the bilayer, the

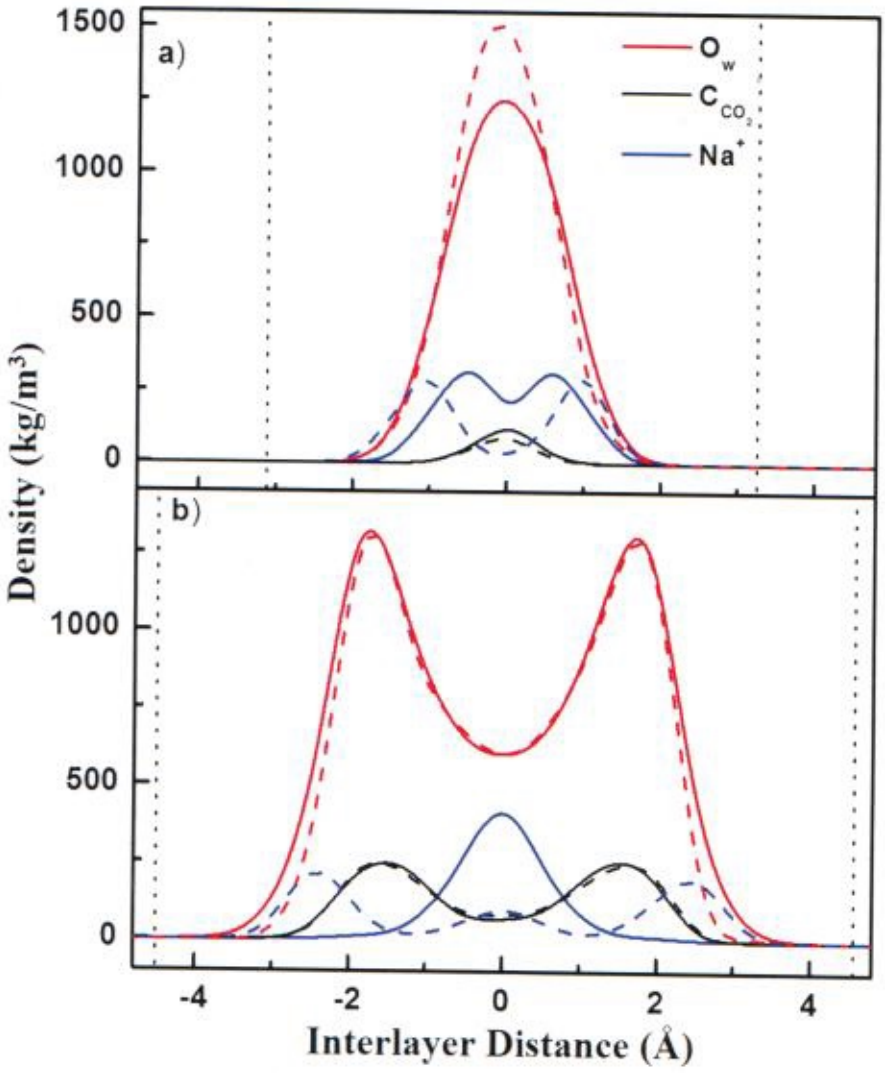

Fig. 8.7 Density profiles of O_w, C_{CO_2}, and Na^+ along the interlayer distance perpendicular to internal surfaces of MMT (*solid*) and beidellite (*dashed lines*) reported for *d*-spacing. **a** 12.5 Å and **b** 15.5 Å. For **b** C_{CO_2} is magnified by a factor of 10. Vertical *dotted lines* indicate the planes of basal oxygen atoms—reprinted with permission from (Makaremi et al., 2015) Copyright (2015) American Chemical Society

sodium ions in MMT develop a well-defined single peak at the interlayer center indicating the formation of outer-sphere complexes of fully hydrated ions. In beidellite, the ions are predominantly adsorbed at the surfaces forming inner-sphere complexes. Suter et al. (2012) explored the thermodynamics of Li^+, Na^+, and K^+-MMT and beidellite using *ab initio* MD. These authors found that smectites with

the free energy minimum in the middle of the interlayer for bilayer swell to the 2 W hydration state with the ions forming a full hydration sphere. In beidellite, the position of the lowest energy region remains unchanged from a monolayer to bilayer indicating that swelling would tend to stop at monolayer. That is confirmed by the swelling energy curve depicted in Fig. 8.5. Thus, the interplay between the hydration of counter-balancing ions and the attraction to the basal surface determines the swelling behavior of smectites. Localization of charge in the octahedral sheets supports swelling to 2 W (and higher) while isomorphic substitutions in the tetrahedral sheets favor 1 W (Figs. 8.5 and 8.7).

Rao and Leng (2016a, b) reported the effect of layer charge, including the influence of charge amount and charge location, on the intercalation of the carbon dioxide–water mixture in Na-MMT clay interlayers under typical CO_2 geologic sequestration conditions (T = 323 K, P = 90 bar). For the two clay models used in the study, one possessed layer charge of −1.0 *e*/unit cell ("high-charge") in the octahedral sheets only, and the other one had −0.75 *e*/unit cell split between the octahedral (2/3) and the tetrahedral sheets (1/3) ("low-charge"). Using MC and MD simulations they explored the effect of layer charge under variable RH following the recent experimental studies that demonstrated exposure of dry supercritical CO_2 to MMT samples in the 2 W and higher hydration states can induce a collapse of the d_{001}-spacing to that of the 1 W state (Ilton et al., 2012; Schaef et al., 2012). On the other hand, the interaction of those samples with wet $scCO_2$ promotes swelling of smectites to either 1 W or 2 W hydration states (Rother et al., 2013; Ilton et al., 2012; Schaef et al., 2012).

Figure 8.8 demonstrates the changes of the d_{001}-spacing and intercalated amount of carbon dioxide in the interlayer as functions of RH for "high-charge" and "low-charge" models. The simulated data are compared against experimental results reported by Loring et al. (2014) at the same pressure and temperature conditions. The

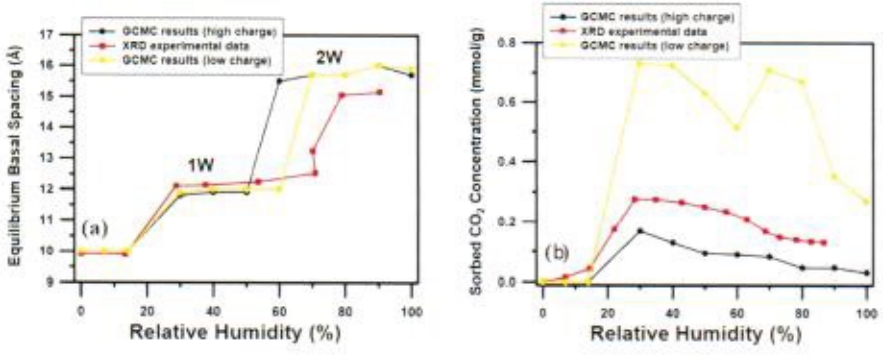

Fig. 8.8 Variations of **a** equilibrium basal spacing and **b** adsorbed CO_2 concentration as a function of RH for the high- and low-charge Na-MMT at T/P = 323 K/90 bar. XRD and IR experimental data obtained by Loring et al. (2014) are shown for comparisons—reprinted with permission from (Rao & Leng, 2016a) Copyright (2016) American Chemical Society

1 W-to-2 W transition occurs at a lower RH in the "high-charge" clay than in the "low charge" one. This 1 W-to-2 W swelling of the high-charge clay is consistent with experimental results (Sato et al., 1992; Michot et al., 2005) and is associated with greater ability of the "high-charge" clay to accommodate water uptake.

Subsequently, "high-charge" clay minerals contain more water and less CO_2 as the RH increases because of the increased number of interlayer cations and the strong hydration energy of sodium ions with polar water molecules. This enhanced hydration process reduces the chances of intercalation of nonpolar CO_2 molecules. The measured adsorbed CO_2 falls in between the "high-charge" and "low-charge" clay-model predictions confirming the importance of the amount of charge and its localization on the intercalation process at variable RH.

The chemical nature of the counter-balancing ions affects the CO_2 intercalation indirectly because CO_2 is not largely participating in the first hydration shell of those ions (Rao & Leng, 2016b; Kadoura et al., 2016; Makaremi et al., 2015; Sena et al., 2015; Botan et al., 2010) due to cation-H_2O interactions are on average ~30% stronger than cation–CO_2 interactions (Criscenti & Cygan, 2013). Differently charged ions, particularly mono- and divalent cations (like Li^+, Na^+, K^+, and Ca^{2+}, Mg^{2+}, respectively) provide different hydration mechanisms with strong implications to the interlayer structure and the ability of swelling clays to retain CO_2. Generally, smectite clay minerals containing divalent interlayer cations require less H_2O saturation to achieve the same d_{001}-spacing values compared to those containing monovalent cations (Ferrage, Lanson, Sakharov, & Drits, 2005; Loganathan et al., 2016). Loring et al. (2014) and Schaef et al. (2015) used a combination of experimental tools to explore CO_2 intercalation into hydrated Na-, Ca-, and Mg-exchanged MMT. They found that Ca-MMT with residual water content (0 W or sub-1 W hydration states) adsorbs almost three times more (1.26 vs. 0.45 mmol/g clay) CO_2 than Na-MMT. The numbers account for non-interlayer adsorption and, assuming similar external surfaces for both clay samples, the difference is primarily due to CO_2 intercalation. The greater ability of smectites with divalent cations to accommodate CO_2 can be associated with a fewer number of those cations per unit cell and their stronger interaction with water molecules comparing to monovalent counterparts. That means less steric hindrance for CO_2 to enter the interlayer, which is facilitated by the larger ionic radii of the divalent cations. This results in propping open the interlayer at near 0 W hydrate states and larger basal d_{100}-spacings (Giesting et al., 2012a; Schaef et al., 2015).

Recently, Michels et al., (2015) studied intercalation of CO_2 in synthetic dried fluorohectorites (representing a "homogeneous" model of natural smectites) with Li^+, Na^+, and exotic Ni^{2+} as counter-ions using X-ray diffraction measurements at −20 °C and 20 bar. Upon exposure to CO_2 the Ni-fluorohectorite develops two distinct diffraction peaks corresponding to d_{001}-spacing at 1.219 and 1.311 nm in contrast to Li- and Na- fluorohectorites demonstrating a well-defined peak at 1.196 and 1.240 nm, respectively. For Ni-fluorohectorite, the peak at 1.311 nm falls between the interlayer distances corresponding to 1 W and 2 W hydration states

(Ferrage et al., 2005, 2011). The author speculated that the unusual (001) diffraction can be attributed to the formation of a CO_2-Ni^{2+} complex in the interlayer and possible interference of a brucite-like structure ($Ni[OH]_2$) (Michels et al., 2014). A theoretical study inspired by these results could be a valuable tool to interpret such observed phenomena.

8.2 Carbon Dioxide and Wettability of Clay Mineral Surfaces

As noted above, the interaction of CO_2 with clay mineral surfaces is expected to be a key process for evaluating the suitability of carbon sequestration to reduce atmospheric carbon emissions and mitigate global climate change. Although the interlayer of swelling clay minerals can potentially provide secondary storage for CO_2 in isolating the greenhouse gas from the environment, the primary interactions during injection and subsequent flow of supercritical CO_2 fluid into the subsurface are the CO_2 fluid interactions with aqueous brine and with external mineral surfaces associated with the reservoir rock and overlying shale caprock. The relative wetting of pore surfaces in the rock matrix by CO_2 and brine will determine the capillary pressure of the fluids, their subsequent transport in the rock matrix, and the ultimate distribution of CO_2 in the reservoir. The integrity of the shale caprock will depend in part on the wettability of CO_2 on the external surfaces of the predominant clay minerals. The relative wetting of pore surfaces is characterized macroscopically by contact angles and interfacial tensions among the three phases (CO_2, brine, and mineral) and which ultimately control the capillary flow and trapping of CO_2 in the rock matrix. This residual trapping mechanism for CO_2 dominates during fluid injection and CO_2 migration stages of carbon sequestration (up to approximately 100 years) and is accompanied by solubility trapping (dissolution of CO_2 into brine) and later (10–10,000 years) by enhanced mineral trapping involving the precipitation of carbonate minerals (Benson et al., 2005).

A molecular basis for the analysis of CO_2-brine-mineral contact angles can be useful in evaluating multiphase flow and the role of residual trapping mechanisms in carbon sequestration. Large-scale molecular dynamics simulations can provide significant insight into competitive wetting of fluids on clay mineral surfaces, especially in view of the large variability of experimental measurements of contact angles which is typically attributed to sample preparation, surface contamination, surface roughness, hysteresis, and other practical issues (Iglauer, Pentland, & Busch, 2015). Simulations of contact angle models involve the equilibration of a large droplet, comprised of many tens to hundreds of thousand fluid molecules (CO_2 or H_2O, or brine) in the coexisting fluid, onto a mineral surface under the appropriate *P*/*T* conditions. Competition between fluids in wetting of the mineral surface ultimately leads to redistribution of fluid molecules and solutes at the

three-phase interface. Also, unique in the contact angle simulations involving CO_2 and H_2O fluids for carbon sequestration applications is the relative significance of polar molecules and the degree to which the molecules interact with various clay mineral surfaces (Tenney & Cygan, 2014; Chen et al., 2016). Other molecular simulation studies that have examined contact angle involving mineral substrates include epoxy on SiO_2 (Hölck et al., 2012), CO_2 and brine on quartz (Iglauer, Mathew, & Bresme, 2012), and water on kaolinite (Šolc, Gerzabek, Lischka, & Tunega, 2011). Often the second "fluid" in many such studies is simply a vacuum. Molecular models to determine interfacial tensions for CO_2-H_2O systems have been developed by Nielsen, Bourg, & Sposito, (2012) and Li et al., (2013).

Figure 8.9 includes a snapshot of an equilibrated supercritical CO_2 droplet in water on the hydroxylated basal surface of kaolinite, obtained after more than 10 ns of molecular dynamics simulation, and which involves more than a half million atoms (Tenney & Cygan, 2014). Corresponding atomic density maps for water derived from equilibrated simulation of pure water, and from similar simulations for CO_2 droplets in NaCl and $CaCl_2$ brine solutions, are also presented. The equilibrium contact angle of 169 ± 63 ° is observed for the case of CO_2 droplet in water and represents the strong interaction with water and the formation of hydrogen bonds with the aluminol groups (-AlOH) of the basal surface; that is, the water phase prefers contact with the clay surface while the CO_2 droplet behaves as a nonwetting fluid. The corresponding water density map shows the uniform ordering of the first surface water layer and a somewhat less-ordered second water layer. The latter exhibits some disruption immediately below the CO_2 droplet; simulations involving such hydrophilic surfaces typically exhibit two to three water layers intermediate between the mineral and the CO_2 droplet. The researchers observed contact angles $31 \pm 6°$ for the case of CO_2 droplet in water on the basal siloxane surface of kaolinite. The siloxane surface of kaolinite is hydrophobic due to limited localized charge associated with the silicate framework and absence of surface hydroxyl groups.

Atomic density maps for the brine components derived from the equilibrated contact angle simulations exhibit compositional distributions consistent with nonwetting CO_2 droplets (i.e., contact angles of 180°). No significant distinction in droplet configuration is observed between NaCl and $CaCl_2$ brines although there is a difference in the distribution of the two cations at the CO_2-brine and brine-kaolinite interfaces. In particular, monovalent Na^+ forms primarily inner-sphere adsorption complexes on the hydroxylated kaolinite surface while divalent Ca^{2+} occurs mostly as an outer-sphere complex. Distributions of both cations directly below the CO_2 droplets are less uniform in the thin film of intermediate water than in the bulk water. Calcium concentration appears slightly enhanced in the brine at the margins of the CO_2 droplet. Chloride exhibits primarily inner-sphere adsorption behavior in both brines at the kaolinite surface. Although the molecular underpinning of wettability is not fully understood for complex natural samples, the use of molecular simulation provides some helpful insights into the fundamental interactions that control the competition of fluids in wetting idealized clay mineral surfaces.

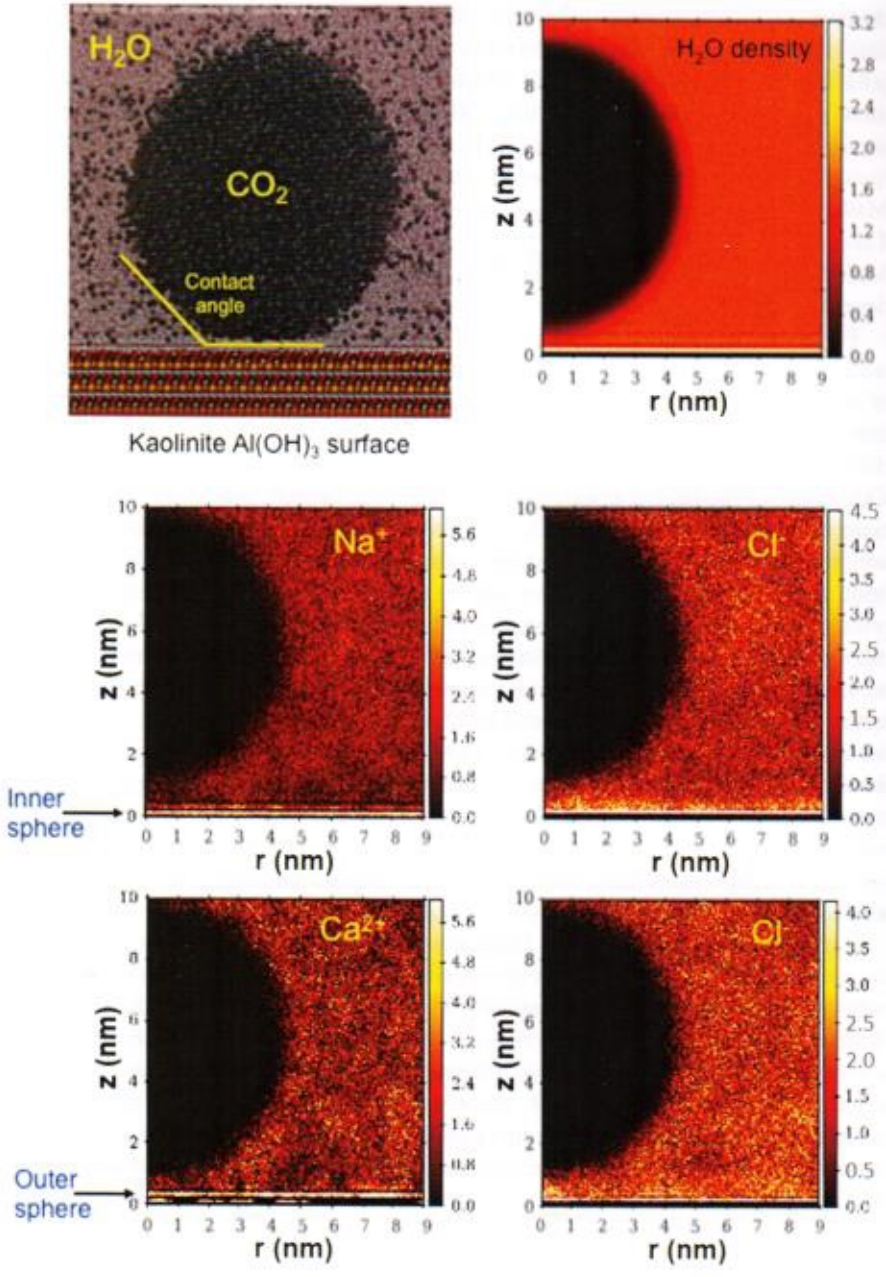

Fig. 8.9 Snapshot of an equilibrated supercritical CO_2 droplet in water at 330 K and 20 MPa on the hydroxylated basal surface of kaolinite, obtained by MD simulation; corresponding atomic density maps for water derived from equilibrated simulation of pure water (*upper right*) and for brine components from equivalent simulations for CO_2 droplets in NaCl and $CaCl_2$ brine solutions (*below*). Reprinted with permission from (Tenney & Cygan, 2014) Copyright (2014) American Chemical Society

8.3 Methane and Swelling Clay Minerals

The interaction of methane with swelling clay has mainly focused on the intercalation of gas hydrates into the interlayer of 2:1 phyllosilicate minerals (Martos-Villa et al., 2014). The high pressure (>20 bar) and relatively low temperature (273–290 K) (Sloan & Koh, 2008; Davie, Zatsepina, & Buffett, 2004; Sun & Duan, 2007) required to form methane hydrate imply that hydrate formation within the interlayer could occur in permafrost areas and the sub-sea surface sediments near continental margins (Milkov, 2000; Kvenvolden, 1998). A unit cell of the stable structure I methane hydrate consists of 46 water molecules per eight gas molecules, which are encapsulated by two small dodecahedral 5^{12} (20 water molecules) and six large tetrakaidecahedral $5^{12}6^2$ (24 water molecules) cages formed by a three-dimensional water molecule network (Sloan & Koh, 2008). The molar fraction of methane (0.148) in such ice-like hydrate phases is significant compared to its solubility in liquid water (2.82×10^{-5}, at 273.15 K and 10 MPa, Peng-Robinson EoS). Worldwide the total gas-in-place (GIP) in a form of hydrate is an enormous amount. Researchers have reported global GIP estimates of $1–1.75 \times 10^{17}$ ft^3 ($3–5 \times 10^{15}$ m^3; 1.5–2.6 $\times$ 10^3 GtC) (Milkov, 2000); 7×10^{17} ft^3 (2.0×10^{16} m^3; 1×10^4 GtC) (Kvenvolden, 1998); 4.2 x10^{18} ft^3 (1.2×10^{17} m^3; 6.4×10^4 GtC) (Klauda & Sandler, 2002) with most hydrate bound in unconsolidated mud generally dominated by clay minerals. Smectites are commonly present on the ocean floor, at continental margins and oceanic ridges (Chamley, 1997) and, therefore, they can host intercalated hydrates. Although gas trapping within expandable clay structures might contribute to the total resource potential, clay-bound hydrates are outside of technically recoverable resources because of the low sediment permeability resulting in low gas flow rates from dissociating hydrates (Boswell & Collett, 2011).

Generally, the presence of clay-based sediments reduces induction time and alters the mechanism of gas hydrate nucleation and growth relative to that in bulk water phase. This suggests prompt hydrate formation under condition of active gas transport into the interlayer region and to the interface between the liquid phase and a growing hydrate phase (Sloan & Koh, 2008; Myshakin, Jiang, Warzinski, & Jordan, 2009; Thompson et al., 2006). Methane hydrate formation experiments in sediments containing quartz grains mixed with kaolinite (non-swelling clay) confirmed highly uniform character of hydrate saturation throughout the samples. In contrast, control tests without clay present resulted in patchy non-uniform hydrate distribution (Ryan, 2012). A series of laboratory scale experiments in test sediment beds of silica sand has shown that particle size distribution plays an important role in hydrate formation, and available void spaces not filled with water increase the hydrate formation kinetics (Linga et al., 2009; Zhou, Castaldi, & Yegulalp, 2009; Bagherzadeh, Moudrakovski, Ripmeester, & Englezos, 2011). On the other hand, based on experiments performed in stirred tank reactors, it was found that the presence of bentonite clay (1 and 5 wt%) in silica sand with different water saturation levels can inhibit hydrate growth rate (Kumar, Sakpal, Roy, & Kumar, 2015). Reduction in hydrate conversion rate was attributed to either poor mass transfer of

(a)

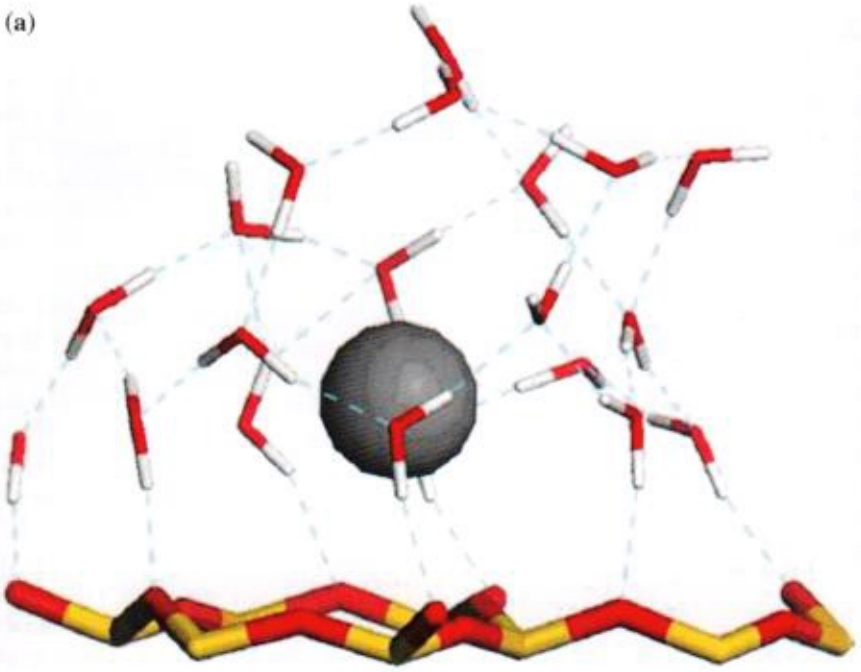

(b)

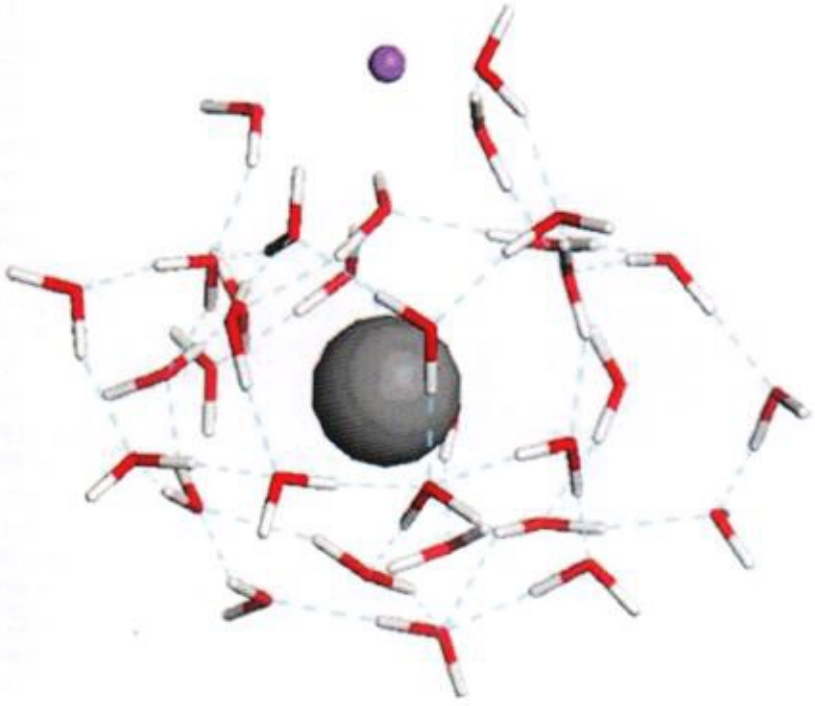

◂**Fig. 8.10** Distorted hydrate cage formed around a methane molecule with participation of **a** interlayer water molecules and basal clay surface, and **b** interlayer water only. *Large spheres* indicate CH_4 molecules; *dashed lines* represent hydrogen bonds; *small sphere* indicates Na^+ ion; *white* and *red* (color version) sticks indicate H and O atoms; yellow sticks indicate Si atoms of MMT (Yan et al., 2014) with permission of Springer

hydrate-forming gases due to the clay swelling (resulting in lower pore sizes) or due to unavailability of free water in silica sand pores.

Experimentally, Guggenheim and Koster van Groos (2003) and Koster van Groos and Guggenheim (2009) reported methane hydrate complexes intercalated between the 2:1 layers of Na-exchanged MMT. The intercalated phase is characterized by a strong ~22 Å peak and a weak second-order ~11 Å diffraction. Given the lattice parameter of structure I methane hydrate is about ~12 Å (Sloan & Koh, 2008) the d_{001}-spacing of 22 Å suggests just enough space to intercalate a hydrate cell unit. Cygan et al. (2004a) performed MD simulations to confirm that a structure similar to methane hydrate is stable in the interlayer of MMT with d_{001}-spacing consistent with experiment as observed by Guggenheim and Koster van Groos (2003). Later, Martos-Villa et al. (2014) revisited the Na-MMT model with intercalated methane hydrate using a larger supercell and adding Na-beidellite to explore the effect of charge localization on likelihood of hydrate formation. The results revealed that predominant isomorphic substitutions in the tetrahedral layers of beidellite weaken the stability of hydrate complex compared to MMT. Based on experimental and simulation data the authors concluded that the intercalated hydrate formation depended on the swelling properties of smectites. Divalent cations like Mg^{2+}, Ca^{2+} or monovalent K^+ (in interstratified illite/smectite) inhibit hydrate formation in the interlayer but rather promote it in the interstitial space of clay particles and on the external clay surfaces.

Hydrogen bond network evolution to encapsulate methane molecules in the interlayer were investigated by many authors (Yan et al., 2014; Martos-Villa et al., 2014; Cygan et al., 2004a; Park & Sposito, 2003). The MC and MD simulations performed to study the stable interlayer CH_4 hydrate structures in Na-MMT demonstrated that methane molecules are stabilized above the hexagonal rings of basal clay surfaces and are surrounded by cage-like water network (Park & Sposito, 2003). Yan et al. (2014) studied methane hydrate formation in MMT with one to eight water layers using Clayff (Cygan et al., 2004b), SPC (Berendsen, Postma, Gunsteren, & Hermans, 1981), and OPLS (Jorgensen, Maxwell, & Tirado-Rives, 1996) force fields to examine the clay phase, water, and methane molecules, accordingly under hydrate forming conditions (260 K and 50 MPa). The simulations demonstrate that hexagonal Si-O ring structure of the clay basal surface can participate in formation of distorted cages around CH_4 together with interlayer water molecules by substituting for some of the cage vertices (Fig. 8.10). The interlayer Na^+ ions can occupy the sites of the network to further distort the hydrate cages making them more irregular compared to the ideal bulk hydrate structure. Consequently, the hydrate formation is facilitated in pores sizes equal to integer or half-integer numbers of hydrate unit cells.

The thermodynamic phase diagram of hydrates in pores impacted by either clay surfaces or other surface materials could be significantly different from that of bulk hydrates. Thermodynamics of the confined hydrates with respect to pore size, geometry, and surface chemistry were studied for the case of a silica gel matrix (Handa & Stupin, 1992; Uchida, Ebinuma, & Ishizaki, 1999; Seo, Lee, & Uchida, 2002). These studies show that confined hydrates dissociate at pressures 20–100% higher than that measured in the bulk phase at the same temperature. This suggests that confined hydrates were much less stable due to nonideal cage structures in the hydrate lattice. Chakraborty and Gelb, (2012) utilized MC simulations to predict dissociation temperatures of methane hydrate crystals inside carbon-like slit-shaped pores. Utilizing the TIP4P (Jorgensen et al., 1983) and TIP4P/2005 (Abascal & Vega, 2005) potentials for water molecules they found that dissociation temperatures are depressed proportionally to the inverse of the pore width following the Gibbs–Thomson equation. Importantly, this behavior is observed for pores small enough that only half-cages of the hydrate structure can fit.

The structure and dynamics of the water-methane binary mixture in the interlayer space of MMT were performed by Rao, Xiang, and Leng, (2013) and Rao and Leng (2014) using grand canonical MC simulations at pressure and temperature conditions beyond the hydrate stability zone. The researchers found that at elevated T and P (T = 460 K and P = 900 bar) mimicking the deep underground geologic conditions at 6 km, methane can enter clay interlayer starting from a single hydration layer (Rao et al., 2013). Methane content in clay increases in a stepwise fashion as the basal spacing increases following the formation of multiple hydration layers. The mole fraction of methane remains low and only slightly increases from 0.03 to 0.05 as the basal spacing increases from 16 to 24 Å. The results show that water density in the interlayer decreases with the increase of temperature and pressure consistent with previous reports (de Pablo, Chavez, & de Pablo, 2005; Cygan et al., 2004a). For example, at basal spacing equal to 16 Å, the number of water molecules in the 8-unit cell MMT system drops from 84.1 at T = 298 K and P = 1 bar (Cygan et al., 2004a) to 66.9 at T = 460 K and P = 900 bar (Rao et al., 2013). The presence of methane insignificantly reduces that number to 63.9. On the other hand, charge localization and extent of substitutions in clay structure remarkably affect the behavior of methane hydration and hydration number (Zhang & Choi, 2006; Zhou et al., 2011). In a subsequent study, Rao and Leng (2014) studied methane intercalation into MMT at 300 K and 20–50 bar corresponding to near-surface geologic conditions (Rao et al., 2013). The results show that methane is incapable of entering the interlayer under the saturated water pressure compared to the previous results obtained at 460 K and 900 bar (Rao et al., 2013). RH within the range of 5–30% are reported to be suitable conditions for methane intercalation. The simulations demonstrated that sodium ions are fully hydrated under the range of RH considered while methane is under hydrated having 40–80% of the total hydration number in bulk phase. Analysis of the radial distribution functions indicates that low RH and the hydrophobic nature of methane leads to condensation of methane into dimers in the interlayer space of the swelling clay minerals. The self-diffusion coefficients of methane characterizing the motion parallel to clay

surface are around 10^{-8}–10^{-9} m^2/s with a tendency to decrease with the increase of RH and pressure (at the same temperature). These numbers are in general agreement with methane diffusion in Na-MMT estimated by Titiloye and Skipper (2001) who used MD simulations under similar pressure and temperature conditions. Later, the same authors studied transport properties of methane in hydrated K-MMT and found the diffusion coefficients and dynamics of methane molecules are comparable with the corresponding Na-MMT system (Titiloye & Skipper, 2005).

8.4 Mixture of Carbon Dioxide and Methane in Swelling Clay Minerals

In practical applications like enhanced gas recovery and CO_2 storage in depleted natural gas reservoirs, there is a complex interaction between H_2O, CO_2 and CH_4 molecules (Chaps. 3 and 6). A shale reservoir is typically characterized with natural fracture and pore networks in a rock matrix. The behavior of fluids in those networks and their interactions with minerals control gas storage and release in a shale matrix, influence transport in the fracture network, and ultimately determine production from unconventional reservoirs. Beside intercalation in swelling clays, CO_2 may preferentially adsorb in nanopores, particularly in (organic) kerogen and on (inorganic) external clay surfaces, and displace CH_4 in shale (Nuttall, Ebble, Drahovzal, & Bustin, 2005). Moreover, free and bound (immobile) water can substantially change the behavior of CH_4 and CO_2 trapped in a shale matrix (Godec, Koperna, Petrusak, & Oudinot, 2013).

Grand canonical (μVT) MC simulations of methane and carbon dioxides intercalation in clay minerals and the effect of water on adsorption behavior of CH_4 and CO_2 in pore space of pyrophyllite and Na-MMT have been investigated (Jin & Firoozabadi, 2013, 2014). The adsorption behavior of the CO_2/CH_4 mixture in Na-MMT was studied using GCMC simulations for ranges of pressures, bulk compositions, and pore sizes (Yang, Liu, & Yang, 2015). The authors have calculated the strength of clay surface interaction with CO_2 (as the isosteric heat of adsorption at nearly zero adsorption loading of a single component) to be 55.4 kJ/mol and 40.5 kJ/mol at 14.0 Å and 20.6 Å of basal d-spacings, respectively. For methane, the corresponding values are 18.9 kJ/mol and 12.5 kJ/mol at 14.0 Å and 20.6 Å, respectively, in agreement with the experimental value (16.0 kJ/mol) for CH_4 adsorption in the pillared clays (Pereira, Pires, & de Carvalho, 2001). Figure 8.11 displays the adsorption isotherms for the binary CO_2/CH_4 mixtures intercalated in Na-MMT as a function of molar fraction of CO_2 in bulk phase composition at the pressures of 0.1 MPa and 1.0 MPa.

The figure shows that as the bulk phase CO_2 molar fraction approaches 0.5 the intercalated methane level converges nearly to zero. The selectivity parameter expressed as $(x_{CO_2}/x_{CH_4})/(y_{CO_2}/y_{CH_4})$ where x and y are mole fractions of two species in adsorbed and bulk phases, respectively, and calculated at 14.0 Å d-spacing can be above 90, while at 20.6 Å the value changes from 25 to 70

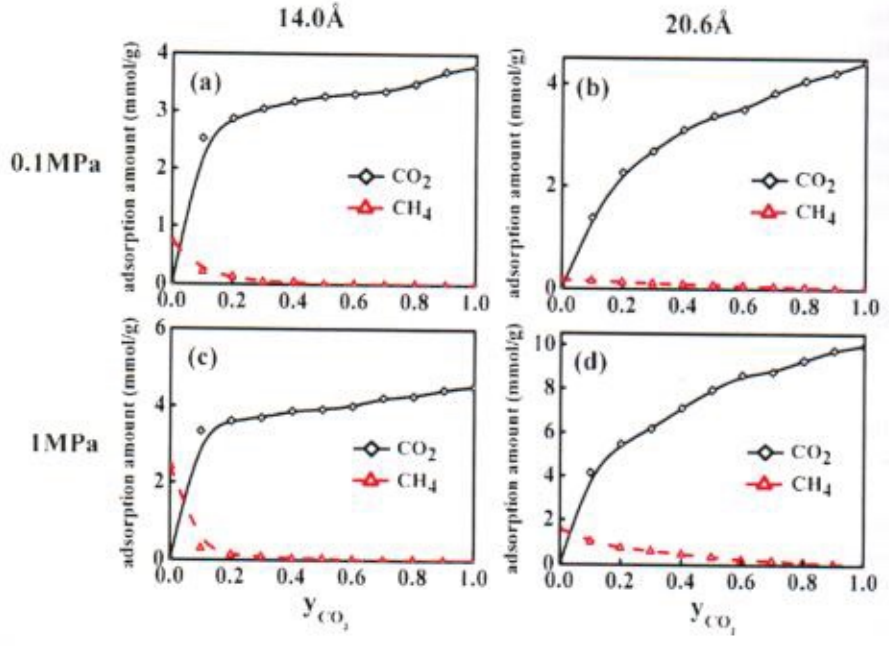

Fig. 8.11 Adsorption isotherms of CO_2/CH_4 mixtures plotted versus mole fraction of CO_2 in bulk phase, for the following examples of gas pressure and basal spacing of Na-MMT: **a** 14.0 Å and **b** 20.6 Å—at 0.1 MPa; **c** 14.0 Å and **d** 20.6 Å—at 1.0 MPa—reprinted from (Yang et al., 2015) with permission from Elsevier

depending on pressure and bulk composition. The greater selectively at the smaller interlayer spacing is attributed to stronger CO_2 interaction with clay surfaces in a more confined environment compared to methane molecules as inferred from the strengths of clay surface interactions given above. The swelling clay demonstrates a substantially higher CO_2 selectivity over methane adsorption indicating that CO_2 molecules competitively replace CH_4 molecules within the interlayer space. This suggests that geological storage of CO_2 in shales (Kulga, Dilmore, Wyatt, & Ertekin, 2014) where clay minerals constitute a significant portion of inorganic matter can induce production of an additional methane volume. Recently, CH_4 adsorption isotherms were measured in clay-dominated rocks to show that the clay mineral composition and the micropore structure significantly affect gas adsorption (Zhang et al., 2012). MMT-rich samples, exhibiting internal surfaces for adsorption, display the highest CH_4 adsorption capacity (Zhang et al., 2012). The additional volume of methane for enhanced gas production also depends on total organic content and the adsorption of CO_2/CH_4 on external surfaces of pores in rock matrix and natural fracture walls. Those results suggest that competitive adsorption/desorption processes should be accounted for in mixed-gas isotherms (Mohammad, Arumugam, Robinson, & Gasem, 2012; Sudibandriyo, Mohammad, Robinson, & Gasem, 2011). Use of mixed-gas isotherms allow more realistic predictions of gas

mixture behavior in shales, which is extremely complex in nature. Another important consideration is the ability of CO_2 molecules exhibit multilayer adsorption. In that case, instead of a Langmuir isotherm implying a monolayer coverage a BET isotherm should be used. For example, Vermylen (2011) studied CO_2 adsorption on crashed and dried Barnett shale samples and found that experimental data are best described by BET isotherms.

References

Abascal, J. L. F., & Vega, C. (2005). A general purpose model for the condensed phases of water: TIP4P/2005. *Journal of Chemical Physics, 123*(234505), 1–12.

Aimoli, C. G., Maginn, E. J., & Abreu, C. R. A. (2014). Transport properties of carbon dioxide and methane from molecular dynamics simulations. *Journal of Chemical Physics, 141*(13), 134101.

Bagherzadeh, S. A., Moudrakovski, I. L., Ripmeester, J. A., & Englezos, P. (2011). Magnetic resonance imaging of gas hydrate formation in a bed of silica sand particles. *Energy & Fuels, 25*(7), 3083–3092.

Benson, S. M., & Cole, D. R. (2008). CO_2 sequestration in deep sedimentary formations. *Elements, 4*(5), 325–331.

Benson, S. M., et al. (2005). Underground geological storage. In B. Metz et al. (Eds.), *IPCC special report on carbon dioxide capture and storage* (Chap. 5, pp. 195–276). Cambridge and New York: Cambridge University Press.

Berendsen, H. J. C., Postma, J. P. M., Gunsteren, W. F., & Hermans, J. (1981). Interaction models for water in relation to protein hydration. In B. Pullman (Ed.), *Intermolecular forces. The Jerusalem symposia on quantum chemistry and biochemistry* (B 14, pp. 331–342). Dordrecht: Springer.

Billemont, P., Coasne, B., & De Weireld, G. (2010). An experimental and molecular simulation study of the adsorption of carbon dioxide and methane in nanoporous carbons in the presence of water. *Langmuir, 27*(3), 1015–1024.

Boswell, R., & Collett, T. S. (2011). Current perspectives on gas hydrate resources. *Energy and Environmental Science, 4*, 1206–1215.

Botan, A., et al. (2010). Carbon dioxide in montmorillonite clay hydrates: Thermodynamics, structure, and transport from molecular simulation. *Journal of Physical Chemistry C, 114*(35), 14962–14969.

Burgess, J. (1999). *Ions in solution: Basic principles of chemical interactions* (1st ed.). Cambridge: Woodhead Publishing.

Chakraborty, S. N., & Gelb, L. D. (2012). A monte carlo simulation study of methane clathrate hydrates confined in slit-shaped pores. *Journal of Physical Chemistry B, 116*(7), 2183–2197.

Chamley, H. (1997). Clay mineral sedimentation in the ocean. *Soils and sediments* (pp. 269–302). Berlin: Springer.

Chen, C., et al. (2016). Pressure and temperature dependence of contact angle for CO_2/water/silica systems predicted by molecular dynamics simulations. *Energy & Fuels, 30*(6), 5027–5034.

Cipriani, P., Nardone, M., Ricci, F. P., & Ricci, M. A. (2001). Orientational correlations in liquid and supercritical CO_2: Neutron diffraction experiments and molecular dynamics simulations. *Molecular Physics, 99*(4), 301–308.

Criscenti, L. J., & Cygan, R. T. (2013). Molecular simulations of carbon dioxide and water: Cation solvation. *Environmental Science and Technology, 47*(1), 87–94.

Cygan, R. T., Guggenheim, S., & Koster van Groos, F. (2004a). Molecular models for the intercalation of methane hydrate complexes in montmorillonite clay. *Journal of Physical Chemistry B, 108*(39), 15141–15149.

Cygan, R. T., Liang, J.-J., & Kalinichev, A. G. (2004b). Molecular models of hydroxide, oxyhydroxide, and clay phases and the development of a general force field. *Journal of Physical Chemistry B, 108*(4), 1255–1266.

Cygan, R. T., Romanov, V. N., & Myshakin, E. M. (2012). Molecular simulation of carbon dioxide capture by montmorillonite using an accurate and flexible force field. *Journal of Physical Chemistry C, 116*(24), 13079–13091.

Davie, M. K., Zatsepina, O. Y., & Buffett, B. A. (2004). Methane solubility in marine hydrate environments. *Marine Geology, 203*(1–2), 177–184.

de Pablo, L., Chavez, M. L., & de Pablo, J. J. (2005). Stability of Na-, K-, and Ca-montmorillonite at high temperatures and pressures: A Monte Carlo simulation. *Langmuir, 21*(23), 10874–10884.

Ferrage, E., Lanson, B., Sakharov, B. A., & Drits, V. A. (2005). Investigation of smectite hydration properties by modeling experimental X-ray diffraction patterns: Part I. *Montmorillonite hydration properties. American Mineralogist, 90*(8–9), 1358–1374.

Ferrage, E., et al. (2011). Hydration properties and interlayer organization of water and ions in synthetic Na-smectite with tetrahedral layer charge. Part 2. Toward a precise coupling between molecular simulations and diffraction data. *Journal of Physical Chemistry C, 115*(5), 1867–1881.

Fu, M. H., Zhang, Z. Z., & Low, P. F. (1990). Changes in the properties of a montmorillonite-water system during the adsorption and desoprtion of water: Hysteresis. *Clays and Clay Minerals, 38*(5), 485–492.

Giesting, P., Guggenheim, S., Koster van Groos, A. F., & Busch, A. (2012a). X-ray diffraction study of K- and Ca-exchanged montmorillonites in CO_2 atmospheres. *Environmental Science and Technology, 46*(10), 5623–5630.

Giesting, P., Guggenheim, S., Koster van Groos, A. F., & Busch, A. (2012b). Interaction of carbon dioxide with Na-exchanged montmorillonite at pressures to 640 bar: Implications for CO_2 sequestration. *International Journal of Greenhouse Gas Control, 8*, 73–81.

Godec, M., Koperna, G., Petrusak, R., & Oudinot, A. (2013). Potential for enhanced gas recovery and CO_2 storage in the Marcellus Shale in Eastern United States. *International Journal of Coal Geology, 118*, 95–104.

Guggenheim, S., & Koster van Groos, A. (2003). Experimental investigation of methane gas production from methane hydrate. *Geology, 31*(7), 653–655.

Handa, Y. P., & Stupin, D. (1992). Thermodynamic properties and dissociation characteristics of methane and propane hydrates in 70 Å radius silica gel pores. *Journal of Physical Chemistry, 96*(21), 8599.

Harris, J. G., & Yung, K. H. (1995). Carbon dioxide's liquid-vapor coexistence curve and critical properties as predicted by a simple molecular model. *Journal of Physical Chemistry, 99*(31), 12021–12024.

Heinz, H., Lin, T.-J., Mishra, R. K., & Emami, F. S. (2013). Thermodynamically consistent force fields for the assembly of inorganic, organic, and biological nanostructures: The INTERFACE force field. *Langmuir, 29*(6), 1754–1765.

Hölck, O., et al. (2012). Comparative characterization of chip to epoxy interfaces by molecular modeling and contact angle determination. *Microelectronics Reliability, 52*(7), 1285–1290.

Huber, M. L., 2007. *NIST Thermophysical Properties of Hydrocarbon Mixtures Database (SUPERTRAPP)*. Available online at: https://www.nist.gov/sites/default/files/documents/srd/Supertrapp.pdf. Accessed 8 May 2017.

Hur, T.-B., et al. (2013). Carbonate formation in Wyoming montmorillonite under high pressure carbon dioxide. *International Journal of Greenhouse Gas Control, 13*, 149–155.

Iglauer, S., Mathew, M. S., & Bresme, F. (2012). Molecular dynamics computations of brine-CO_2 interfacial tensions and brine-CO_2-quartz contact angles and their effects on structural and residual trapping mechanisms in carbon geo-sequestration. *Journal of Colloid and Interface Science, 386*(1), 405–414.

Iglauer, S., Pentland, C. H., & Busch, A. (2015). CO_2 wettability of seal and reservoir rocks and the implications for carbon geo-sequestration. *Water Resources Research, 51*(1), 729–774.

Ilton, E. S., et al. (2012). In Situ X-Ray diffraction study of Na^+ saturated montmorillonite exposed to variably wet super critical CO_2. *Environmental Science and Technology, 46*(7), 4241–4248.

Ji, L., et al. (2012). Experimental investigation of main controls to methane adsorption in clay-rich rocks. *Applied Geochemistry, 27*(12), 2533–2545.

Jin, Z., & Firoozabadi, A. (2013). Methane and carbon dioxide adsorption in clay-like slit pores by Monte Carlo simulations. *Fluid Phase Equilibria, 360*, 456–465.

Jin, Z., & Firoozabadi, A. (2014). Effect of water on methane and carbon dioxide sorption in clay minerals by Monte Carlo simulations. *Fluid Phase Equilibria, 382*, 10–20.

Jorgensen, W. L., et al. (1983). Comparison of simple potential functions for simulating liquid water. *Journal of Chemical Physics, 79*(2), 926.

Jorgensen, W. L., Maxwell, D. S., & Tirado-Rives, J. (1996). Development and testing of the OPLS all-atom force field on conformational energetics and properties of organic liquids. *Journal of American Chemical Society, 118*(45), 11225–11236.

Kadoura, A., Nair, A. K. N., & Sun, S. (2016). Molecular dynamics simulations of carbon dioxide, methane, and their mixture in montmorillonite clay hydrates. *Journal of Physical Chemistry C, 120*(23), 12517–12529.

Klauda, J. B., & Sandler, S. I. (2002). Ab initio intermolecular potentials for gas hydrates and their predictions. *Journal of Physical Chemistry B, 106*(22), 5722–5732.

Koster van Groos, A. F., & Guggenheim, S. (2009). The stability of methane hydrate intercalates of montmorillonite and nontronite: Implications for carbon storage in ocean-floor environments. *American Mineralogist, 94*(2–3), 372–379.

Kulga, B., Dilmore, R., Wyatt, C., & Ertekin, T. (2014). *Investigation of CO_2 storage and enhanced gas recovery in depleted shale gas formations using a dual-porosity/dual-permeability, multiphase reservoir simulator*. Morgantown, WV: U.S. Department of Energy.

Kumar, A., Sakpal, T., Roy, S., & Kumar, R. (2015). Methane hydrate formation in a test sediment of sand and clay at various levels of water saturation. *Canadian Journal of Chemistry, 93*(8), 874–881.

Kvenvolden, K. A. (1998). A primer on the geological occurrence of gas hydrate. *The Geological Society, London, Special Publications, 137*, 9–30.

Lee, M. S., McGrail, B. P., & Glezakou, V. A. (2014). Microstructural response of variably hydrated Ca-rich montmorillonite to supercritical CO_2. *Environmental Science and Technology, 48*(15), 8612–8619.

Linga, P., et al. (2009). Gas hydrate formation in a variable volume bed of silica sand particles. *Energy & Fuels, 23*(1), 5496–5507.

Li, X., et al. (2013). Molecular dynamics simulations of CO_2 and brine interfacial tension at high temperatures and pressures. *Journal of Physical Chemistry B, 117*(18), 5647–5652.

Loganathan, N., et al. (2016). Cation and water structure, dynamics, and energetics in smectite clays: A molecular dynamics study of Ca-hectorite. *Journal of Physical Chemistry C, 120*(23), 12429–12439.

Loring, J. S., et al. (2014). In Situ study of CO_2 and H_2O partitioning between Na-montmorillonite and variably wet supercritical carbon dioxide. *Langmuir, 30*(21), 6120–6128.

Lutterotti, L., et al. (2010). Texture analysis of a turbostratically disordered Ca-montmorillonite. *American Mineralogist, 95*(1), 98–103.

Makaremi, M., Jordan, K. D., Guthrie, G. D., & Myshakin, E. M. (2015). Multiphase Monte Carlo and molecular dynamics simulations of water and CO_2 intercalation in montmorillonite and beidellite. *Journal of Physical Chemistry C, 119*(27), 15112–15124.

Martos-Villa, R., et al. (2014). Interaction of methane hydrate complexes with smectites: Experimental results compared to molecular models. *American Mineralogist, 99*(2–3), 401–414.

Michalkova, A., & Tunega, D. (2007). Kaolinite: Dimethylsulfoxide intercalate—A theoretical study. *Journal of Physical Chemistry C, 111*(30), 11259–11266.

Michels, L., et al. (2014). EXAFS and XRD studies in synthetic Ni-fluorohectorite. *Applied Clay Science, 96*, 60–66.

Michels, L., et al. (2015). Intercalation and retention of carbon dioxide in a smectite clay promoted by interlayer cations. *Scientific Reports, 5*(8775), 1–9.

Michot, L. J., et al. (2005). Hydration and swelling of synthetic Na-Saponites: Influence of layer charge. *American Mineralogist, 90*(1), 166–172.

Milkov, A. V. (2000). Worldwide distribution of submarine mud volcanoes and associated gas hydrates. *Marine Geology, 167*(1–2), 29–42.

Mohammad, S. A., Arumugam, A., Robinson, R. L. J., & Gasem, K. A. M. (2012). High-pressure adsorption of pure gases on coals and activated carbon: Measurements and modeling. *Energy & Fuels, 26*(1), 536–548.

Myshakin, E. M., Jiang, H., Warzinski, R. P., & Jordan, K. D. (2009). Molecular dynamics simulations of methane hydrate decomposition. *Journal of Physical Chemistry A, 113*(10), 1913–1921.

Myshakin, E. M., et al. (2013). Molecular dynamics simulations of carbon dioxide intercalation in hydrated Na-montmorillonite. *Journal of Physical Chemistry C, 117*(21), 11028–11039.

Myshakin, E. M., et al. (2014). Molecular dynamics simulations of turbostratic dry and hydrated montmorillonite with intercalated carbon dioxide. *The Journal of Physical Chemistry A, 118* (35), 7454–7468.

Nielsen, L. C., Bourg, I. C., & Sposito, G. (2012). Predicting CO_2-water interfacial tension under pressure and temperature conditions of geologic CO_2 storage. *Geochimica et Cosmochimica Acta, 81*, 28–38.

Nuttall, B., Ebble, C., Drahovzal, J. A., & Bustin, R. M. (2005). *Analysis of Devonian black shales in Kentucky for potential carbon dioxide sequestration and enhanced natural gas production*. Lexington, KY: University of Kentucky.

Park, S.-H., & Sposito, G. (2003). Do montmorillonite surfaces promote methane hydrate formation? Monte Carlo and molecular dynamics simulations. *Journal of Physical Chemistry B, 107*(10), 2281–2290.

Pereira, P. R., Pires, J., & de Carvalho, M. B. (2001). Adsorption of methane and ethane in zirconium oxide pillared clays. *Separation and Purification Technology, 21*(3), 237–246.

Rao, Q., & Leng, Y. (2014). Methane aqueous fluids in montmorillonite clay interlayer under near-surface geological conditions: A grand canonical Monte Carlo and molecular dynamics simulation study. *Journal of Physical Chemistry B, 118*(37), 10956–10965.

Rao, Q., & Leng, Y. (2016a). Effect of layer charge on CO_2 and H_2O intercalations in swelling clays. *Langmuir, 32*(44), 11366–11374.

Rao, Q., & Leng, Y. (2016b). Molecular understanding of CO_2 and H_2O in a montmorillonite clay interlayer under CO_2 geological sequestration conditions. *Journal of Physical Chemistry C, 120*(5), 2642–2654.

Rao, Q., Xiang, Y., & Leng, Y. S. (2013). Molecular simulations on the structure and dynamics of water-methane fluids between Na-Montmorillonite clay surfaces at elevated temperature and pressure. *Journal of Physical Chemistry C, 117*(27), 14061–14069.

Romanov, V. N. (2013). Evidence of irreversible CO_2 intercalation in montmorillonite. *International Journal of Greenhouse Gas Control, 14*, 220–226.

Rother, G., et al. (2013). CO_2 sorption to subsingle hydration layer montmorillonite clay studied by excess sorption and neutron diffraction measurements. *Environmental Science and Technology, 47*(1), 205–211.

Ryan, T. (2012). *Effect of sediment composition on the uniformity of experimentally-formed methane hydrate [MS Thesis]*. Morgantown, WV: West Virginia University, Department of Chemical Engineering.

Saharay, M., & Balasubramanian, S. (2004a). Ab Initio molecular-dynamics study of supercritical carbon dioxide. *Journal of Chemical Physics, 120*(20), 9694–9702.

Saharay, M., & Balasubramanian, S. (2004b). Enhanced molecular multipole moments and solvent structure in supercritical carbon dioxide. *ChemPhysChem, 5*(9), 1442–1445.

Saharay, M., & Dr. Balasubramanian, S. (2006). Errata: Enhanced molecular multipole moments and solvent structure in supercritical carbon dioxide. *ChemPhysChem, 7*(6), 1167.

Sato, T., Watanabe, T., & Otsuka, R. (1992). Effects of layer charge, charge location, and energy change on expansion properties of dioctahedral smectites. *Clays and Clay Minerals, 40*(1), 103–113.

Schaef, H. T., et al. (2012). In situ XRD study of Ca^{2+} saturated montmorillonite (STX-1) exposed to anhydrous and wet supercritical carbon dioxide. *International Journal of Greenhouse Gas Control, 6*, 220–229.

Schaef, H. T., et al. (2015). Competitive sorption of CO_2 and H_2O in 2:1 layer phyllosilicates. *Geochimica et Cosmochimica Acta, 161*, 248–257.

Sena, M. M., Morrow, C. P., Kirkpatrick, R. J., & Krishnan, M. (2015). Supercritical carbon dioxide at smectite mineral–water interfaces: Molecular dynamics and adaptive biasing force investigation of CO_2/H_2O mixtures nanoconfined in Na-montmorillonite. *Chemistry of Materials, 27*(20), 6946–6959.

Seo, Y., Lee, H., & Uchida, T. (2002). Methane and carbon dioxide hydrate phase behavior in small porous silica gels: Three-phase equilibrium determination and thermodynamic modeling. *Langmuir, 18*(24), 9164–9170.

Sloan, E. D., & Koh, C. A. (2008). *Clathrate hydrates of natural gas* (3rd ed.). Boca Raton, FL.: CRC Press.

Smith, D. E., Wang, Y., & Whitley, H. D. (2004). Molecular simulations of hydration and swelling in clay minerals. *Fluid Phase Equilibrium, 222*, 189–194.

Šolc, R., Gerzabek, M. H., Lischka, H., & Tunega, D. (2011). Wettability of kaolinite (001) surfaces—Molecular dynamic study. *Geoderma, 169*, 47–54.

Sudibandriyo, M., Mohammad, S. A., Robinson, R. L. J., & Gasem, K. A. M. (2011). Ono-Kondo model for high-pressure mixed-gas adsorption on activated carbons and coals. *Energy & Fuels, 25*(7), 3355–3367.

Sun, R., & Duan, Z. (2007). An accurate model to predict the thermodynamic stability of methane hydrate and methane solubility in marine environments. *Chemical Geology, 244*(1–2), 248–262.

Suter, J. L., Sprik, M., & Boek, E. S. (2012). Free energies of absorption of alkali ions onto beidellite and montmorillonite surfaces from constrained molecular dynamics simulations. *Geochimica et Cosmochimica Acta, 91*, 109–119.

Tenney, C. M., & Cygan, R. T. (2014). Molecular simulation of carbon dioxide, brine, and clay mineral interactions and determination of contact angles. *Environmental Science and Technology, 48*(3), 2035–2042.

Teppen, B. J., et al. (1997). Molecular dynamics modeling of clay minerals. 1. Gibbsite, kaolinite, pyrophyllite, and beidellite. *Journal of Physical Chemistry B, 101*(9), 1579–1587.

Thompson, H., et al. (2006). Methane hydrate formation and decomposition: Structural studies via neutron diffraction and empirical potential structure refinement. *Journal of Chemical Physics, 124*(16), 164508.

Titiloye, J. O., & Skipper, N. T. (2001). Molecular dynamics simulation of methane in sodium montmorillonite clay hydrates at elevated pressures and temperatures. *Molecular Physics, 99*(10), 899–906.

Titiloye, J. O., & Skipper, N. T. (2005). Monte Carlo and molecular dynamics simulations of methane in potassium montmorillonite clay hydrates at elevated pressures and temperatures. *Journal of Colloid and Interface Science, 282*(2), 422–427.

Uchida, T., Ebinuma, T., & Ishizaki, T. (1999). Dissociation condition measurements of methane hydrate in confined small pores of porous glass. *Journal of Physical Chemistry B, 103*(18), 3659–3662.

Vermylen, J. P. (2011). *Geomechanical Studies of the Barnett Shale, Texas, USA [Ph.D. dissertation]*. Stanford, CA: Stanford University, SRB (Vol. 125).

Viani, A., Gualtieri, A. F., & Artioli, G. (2002). The nature of disorder in montmorillonite by simulation of X-ray power patterns. *American Mineralogist, 87*(7), 966–975.

Yang, N., & Yang, X. (2011). Molecular simulation of swelling and structure for Na-Wyoming montmorillonite in supercritical CO_2. *Molecular Simulations, 37*(13), 1063–1070.

Yang, W., & Zaoui, A. (2016). Capture and sequestration of CO_2 in the interlayer space of hydrated calcium montmorillonite clay under various geological burial depth. *Physica A: Statistical Mechanics and its Applications, 449*, 416–425.

Yang, N., Liu, S., & Yang, X. (2015). Molecular simulation of preferential adsorption of CO_2 over CH_4 in Na-montmorillonite clay material. *Applied Surface Science, 356*, 1262–1271.

Yan, K.-F., et al. (2014). Molecular dynamics simulation of the intercalation behaviors of methane hydrate in montmorillonite. *Journal of Molecular Modeling, 20*(6), 2311.

Young, D. A., & Smith, D. E. (2000). Simulations of clay mineral swelling and hydration: Dependence upon interlayer ion size and charge. *Journal of Physical Chemistry B, 104*(39), 9163–9170.

Zhang, J. F., & Choi, S. K. (2006). Molecular dynamics simulation of methane in potassium montmorillonite clay hydrates. *Journal of Physics B: Atomic, Molecular and Optical Physics, 39*(18), 3839–3848.

Zhang, Z., & Duan, Z. (2005). An optimized molecular potential for carbon dioxide. *Journal of Chemical Physics, 122*(21), 214507.

Zhang, T., et al. (2012). Effect of organic-matter type and thermal maturity on methane adsorption in shale-gas systems. *Organic Geochemistry, 47*, 120–131.

Zhou, Y., Castaldi, M. J., & Yegulalp, T. M. (2009). Experimental investigation of methane gas production from methane hydrate. *Industrial and Engineering Chemistry Research, 48*(6), 3142–3149.

Zhou, Q., et al. (2011). Hydration of methane intercalated in Na-smectites with distinct layer charge: Insights from molecular simulations. *Journal of Colloid and Interface Science, 355*(1), 237–242.

Zhu, A. M., Zhang, X. B., Liu, Q. L., & Zhang, Q. G. (2009). A fully flexible potential model for carbon dioxide. *Chinese Journal of Chemical Engineering, 17*(2), 268–272.